Springer

KSME

Journal of Mechanical Science and Technology 32 (9) (2018) 4201~4208
www.springerlink.com/content/1738-494x(Print)/1976-3824(Online)
DOI 10.1007/s12206-018-0818-0

Determination of creep constitutive model for 28-48WCo alloy based on experimental creep tests at 817-982 °C †

Van Hung Dao[1], Kee Bong Yoon[1], Gimo Yang[2] and Jae Sung Oh[1,*]

[1]*Department of Mechanical Engineering, Chung Ang University, 84 Heukseok-ro, Dongjak, Seoul 06974, Korea*
[2]*MetalLAB Inc., 65 Techno 3-ro, Yuseong, Daejeon 34016, Korea*

(Manuscript Received March 21, 2018; Revised May 29, 2018; Accepted May 30, 2018)

Abstract

The high-chromium high-nickel alloy is widely used as a heat-resistant material for components in plants under elevated temperatures, and thus, prediction of its creep deformation and rupture life is required for safe design. In this study, a creep constitutive model for the 28-48WCo alloy was determined by employing the Sherby-Dorn equation. Creep deformation tests were conducted at temperatures of 817, 871, 927 and 982 °C, under an applied stress ranging from 27.58 to 82.74 MPa. High temperature tension tests were also conducted to measure the change in elastic modulus with temperature variation. The model provided good predictability of the minimum creep strain rate in the range of experimental test conditions, with a coefficient of determination of 0.92. The creep rupture life was characterized using the Larson-Miller parameter. Creep design curves were proposed to estimate the creep rupture life of the 28-48WCo alloy at a temperature range of 817-982 °C.

Keywords: Creep; Rupture life; Constitutive model; Larson-Miller parameter; Fe-Cr-Ni; 28-48WCo

1. Introduction

The 28-48WCo alloy steel belongs to the group of 28 %Cr-48 %Ni heat-resistant stainless steel, with addition of W and Co elements for improving its high temperature mechanical properties. These additive elements increase the heat resistance of the alloy by constraining the precipitation of carbides at grain boundaries and minimizing coarsening of the carbides within the grain [1-4]. The high nickel and chromium contents of the 28-48WCo alloy also make it resistant to corrosion and oxidation at elevated temperatures. Owing to its heat-resisting properties, this alloy has been widely used for components in high temperature chemical plants, such as fittings, castings, and coils in heating furnaces. The 28-48WCo steel is generally used for manufacturing of the above components by conventional casting, while the HK, HP and KHR steels are used for manufacturing furnace tubes by centrifugal casting [5].

The residual life of components manufactured by conventional casting with the 28-48WCo alloy depends on the creep deformation and rupture failure caused by aging and the creep damage accumulated during its service period under high temperature and stress. Thus, reliable predictions of the amount of creep deformation and damage of the 28-48WCo alloy are necessary for safe use of these components.

Various models have been suggested as constitutive equations describing the creep deformation of heat-resisting alloys. The Norton's power law creep model has been one of the most widely used, and the temperature dependency of creep deformation was reliably described by the Arrhenius type model. This approach was successfully employed by Barrett, Ardell, and Sherby [6] for establishing a creep deformation model, which is known as the Sherby-Dorn equation. The power law creep model has been recently applied to describe the creep behavior of the SUS304HV stainless steel using the experimental results of uniaxial creep tests and small punch creep tests, its also applied for alloy 617 in high temperature to study the effect of air and helium environments on the creep behavior [7, 8]. For high Ni-Cr steels, such as the 20Cr-25Ni and HP40Nb alloys, the Sherby-Dorn equation has been applied for modeling creep behavior [9, 10]. A modified Garofalo equation has been applied for the constitutive creep model using the Levenberg-Marquardt algorithm for calculating all coefficients of the creep equation for the P91 steel [11]. The improved Dyson-McLean approach has been also applied for creep deformation behavior of tempered martensitic P9 steel [12]. The concept of continuum damage mechanics (CDM) has been used in this form of creep constitutive equation by considering the load carrying area reduction owing to cavity formation for the 316 stainless steel, 1/2Cr1/2Mo1/4V ferritic

*Corresponding author. Tel.: +82 42 934 0116, Fax.: +82 42 934 0117
E-mail address: janggunab@hanmail.net
† Recommended by Editor Chongdu Cho

Table 1. Chemical composition of the 28-48WCo and KHR48NCo alloys [17, 18] and the material used in this study (wt %).

Material	C	Ni	Cr	Mn	P	S	Co	W	Si	Fe
28-48WCo (required)	0.45-0.50	46.0-50.0	26.0-30.0	≤ 2.0	≤ 0.03	≤ 0.03	2.5-4.0	4.0-6.0	≤ 2.0	Bal
KHR48NCo (required)	0.35-0.65	46.0-50.0	25.0-28.0	≤ 1.5	≤ 0.03	≤ 0.03	2.5-4.5	4.0-6.0	≤ 1.75	Bal
28-48WCo (this study)	0.59	48.84	29.32	1.16	ND	0.01	3.99	5.93	0.50	Bal

steel, 316LN, and HT-9 stainless steels [13-15]. In the Sherby-Dorn equation, the effects of stress and temperature on the creep strain rate are decoupled. In the θ-projection creep model, the effects of temperature and stress are coupled in the constitutive equation. The θ-projection model has been applied for creep behavior of the Cr25Ni35Nb and Cr35Ni45Nb alloys [16].

In this study, the Sherby-Dorn constitutive equation was applied for modeling the creep deformation behavior of the 28-48WCo alloy using experimental creep test results. Creep tests were conducted at temperatures of 817, 871, 927 and 982 °C under a stress range from 27.58 MPa to 82.74 MPa. Further, the creep rupture life data of the same material were modeled with the well-known Larson-Miller parameter.

2. Experimental procedures

2.1 Material and specimens

The conventionally casted 28-48WCo heat resistant stainless steel [17] was used as the test material. The chemical composition of the 28-48WCo required by the manufacturer's specification is listed in Table 1. Because the chemical composition of this material is similar to that of KHR48NCo [18], the composition of the KHR48NCo is also included and compared with that of 28-48WCo. The amounts of C, Cr, Si and Mn are slightly different, and the required amounts of the other components are the same. The 28-48WCo alloy used in this study was produced by conventional casting and its chemical compositions are presented in Table 1.

The tensile and creep test specimens were fabricated following ASTM E8 [19] and ASTM E139 [20] standards by electrical discharge machining. The specimen's diameter and gage length were 6 mm and 30 mm, respectively, and shown in Fig. 1. Specimen for metallurgical investigation was prepared with the as-cast material. The microstructure of the virgin material was investigated using optical microscopy and scanning electron microscopy (SEM). The composition analysis was conducted by energy dispersive x-ray spectroscopy (EDS) analysis.

2.2 Test conditions

The tensile tests were carried out at room temperature and at elevated temperatures of 817, 871, 927 and 982 °C. The tensile strength and percent elongation were measured. From the linear elastic parts of the stress-strain curves, the Young's modulus data were estimated. Creep tests following ASTM E-139 [20] were also conducted at temperatures of 817, 871, 927 and 982 °C in the stress range of 27.58-82.74 MPa. The detailed test conditions are summarized in Table 2. The creep strain-time curves during the tests were recorded. After rupture of the specimens, the failure strain at the gage length of each specimen was measured.

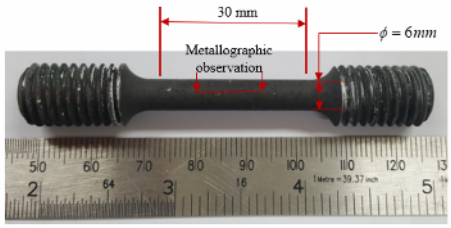

Fig. 1. Specimen before creep testing.

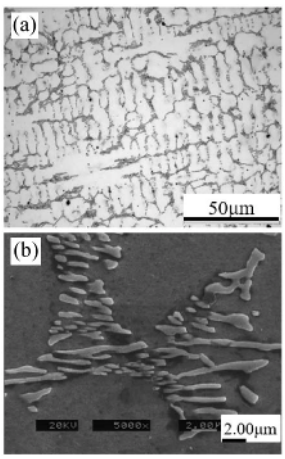

Fig. 2. Microstructure of as-cast 28-48WCo alloy: (a) Optical microscopy at lower magnification (x 400); (b) SEM image at higher magnification (x 5000).

3. Results and discussion

3.1 Microstructure of virgin 28-48WCo alloy

The microstructure of the as-cast 28-48WCo alloy is shown in Fig. 2. The low-magnification image in Fig. 2(a) shows continuous networks of primary carbides appearing as a dendritic pattern formed during solidification. The high magnification in Fig. 2(b) shows carbide precipitates near the grain

Table 2. Creep test results of the conventionally casted 28-48WCo alloy.

Temp. °C (°F)	Applied stress (MPa)	Min. strain rate (h^{-1})	Rupture life (h)	Failure strain (%)
817 (1500)	72.40	6.384E-04	236.04	26.10
	65.50	1.266E-04	523.32	12.35
	58.60	2.287E-05	1372.28	8.84
871 (1600)	82.74	1.487E-02	16.21	46.15
	75.84	6.628E-03	28.77	33.31
	68.95	3.685E-03	50.54	36.31
	62.07	1.073E-03	115.73	19.03
	51.72	2.515E-04	386.33	18.28
	44.82	3.334E-05	1510.28	13.29
927 (1700)	62.05	1.445E-02	14.74	44.00
	55.16	3.216E-03	42.72	26.62
	48.26	1.745E-03	87.86	34.58
	44.82	5.312E-04	177.98	16.49
	41.37	3.467E-04	220.72	17.16
	31.03	3.431E-05	1337.00	14.61
982 (1800)	48.26	1.457E-02	14.69	61.06
	41.37	2.943E-03	43.24	24.05
	34.47	1.016E-03	101.02	22.75
	27.58	2.645E-04	370.05	25.94

boundaries. These precipitates could be identified as chromium carbides (M_7C_3 and/or $M_{23}C_6$ types) and W carbides (M_6C types) based on the EDS analysis results. As shown in Fig. 3, three locations characterizing various carbides were selected and the composition of the carbides was analyzed. At EDS scan locations A and C, in which the precipitates appeared in bright color contrast, Ni and W showed strong peaks that indicated Ni-rich (Ni = 42.69, 45.43 wt.%) and W-rich carbides (W = 8.04, 8.66 wt.%). At EDS scan location B, in which the precipitates appeared as a dark contrasted color, a dominating Cr peak was observed (Cr = 77.87 wt.%), indicating Cr-rich carbides that had been formed during casting. These segregated carbides may affect the material resistance at high temperature.

3.2 Tensile properties

The tensile properties measured with the as-cast 28-48WCo alloy are summarized in Table 3. As the test temperature increased from 817 °C to 982 °C, the tensile strength and Young's modulus decreased. Elongation at failure increased from 22.5 % to 34.0 %, which shows the ductile characteristics of the material. The decrease in tensile strength with increasing operation temperature was explained based on the evolution of carbide precipitates at elevated temperatures [21]. Strength reduction owing to overheating also showed similar microstructural changes, as discussed in Ref. [22]. The Young's modulus, E, decreased rapidly with increasing temperature. It was 207.3 GPa at 817 °C and decreased to 142.3 GPa at 982 °C. Its regression equation was derived, as expressed by Eq. (1), using a second-order polynomial function. The regression accuracy expressed in the root mean square of the error (R^2) was 0.9997.

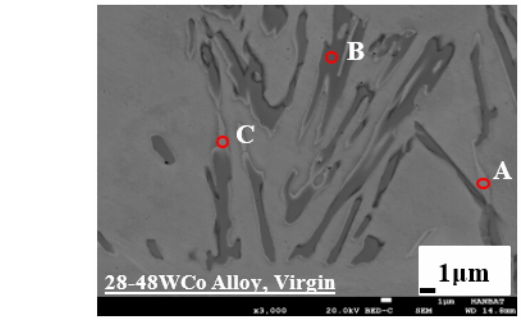

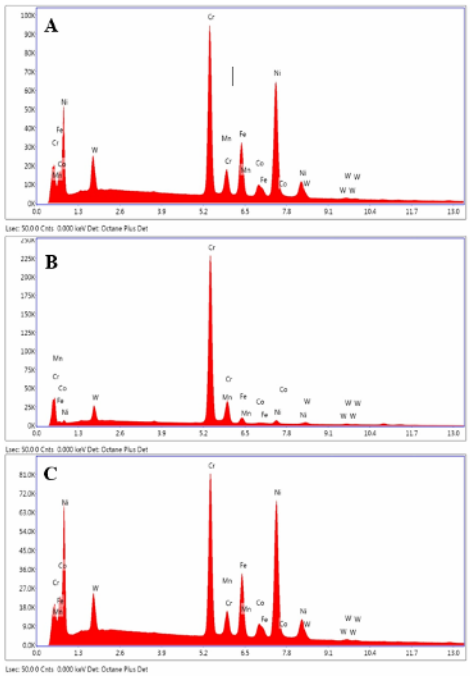

Element	Weight %
Cr K	28.85
Mn K	2.61
Fe K	13.58
Co K	4.25
Ni K	42.69
W L	8.04

Element	Weight %
Cr K	77.87
Mn K	5.73
Fe K	4.96
Co K	1.43
Ni K	3.68
W L	6.33

Element	Weight %
Cr K	24.53
Mn K	2.50
Fe K	14.33
Co K	4.56
Ni K	45.43
W L	8.66

Fig. 3. EDS analysis spectrum of as-cast 28-48WCo alloy.

Table 3. Tensile properties of the conventionally casted 28-48WCo alloy used in this study.

Material	Test conditions °C (°F)	Young's modulus, E (GPa)	Tensile strength, (MPa)	Elongation (%)
28-48WCo alloy	25 (77)	303.4	530.9	10.0
	817 (1500)	207.3	346.3	22.5
	871 (1600)	201.7	276.7	23.3
	927 (1700)	181.0	204.0	27.3
	982 (1800)	142.3	158.3	34.0

$$E(T) = -2.7027\times10^{-3}T^2 + 4.4702\times10^{0}T - 1.6409\times10^{3}. \quad (1)$$

$E(T)$ is Young's modulus in GPa and T is the temperature expressed in °C. This equation was derived using the data in the temperature range of 817-982 °C. The equation can be applied in the 800-1000 °C range with reasonable accuracy.

3.3 Creep properties

The creep test results are summarized in Table 2 and shown in Fig. 4. Fig. 4 shows the creep strain data as a function of the elapsed time in semi-log scales for each test temperature. These creep strain data were converted to creep strain rate data using the 7-point polynomial method of ASTM-E647, shown in Fig. 5 in the log-log scale. Figs. 5(a)-(d) show the strain rate versus elapsed time t at constant temperatures of 817, 871, 927 and 982 °C, respectively, illustrating roughly three creep regimes. The primary creep was scarcely observed and the secondary creep was dominant during the whole creep life. The tertiary creep contribution appeared after half of the creep life. The secondary creep rate, which is the minimum strain rate, was obtained by determining the average value of the strain rate with data in the range of 30-60 % of creep rupture time for each specimen. The obtained minimum strain rate is also summarized in Table 2.

Using the measured secondary creep rate, the Norton's power law creep constants were determined as shown in Fig. 6.

The secondary creep follows the power law creep model rather well. As the temperatures varied as 817, 871, 927 and 982 °C, the power law creep exponent changed as 15.76, 9.68, 8.55 and 6.96, respectively. As the temperature increased, the power law hardening decreased owing to the thermally activated process. It should be noted that the exponent value at 817 °C was considerably high when compared with the other cases.

3.4 Constitutive equation for minimum creep strain rate

The minimum creep strain rate depends on the applied stress (σ) and temperature (T), as shown in Fig. 6. The constitutive equation for creep deformation suggested by Sherby-Dorn, and Barrett et al. [6] was employed in this study. The minimum strain rate can be expressed as a function of (σ, T),

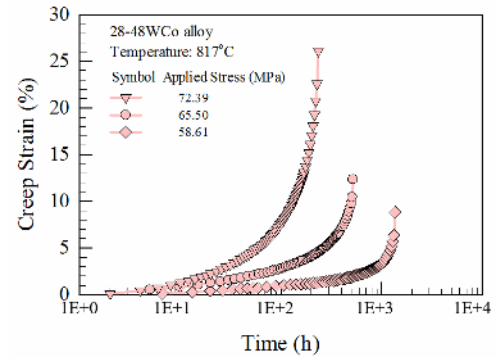

(a)

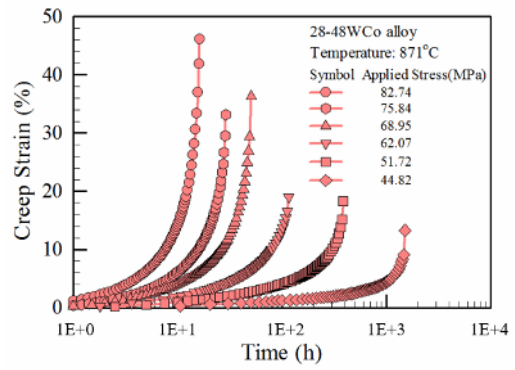

(b)

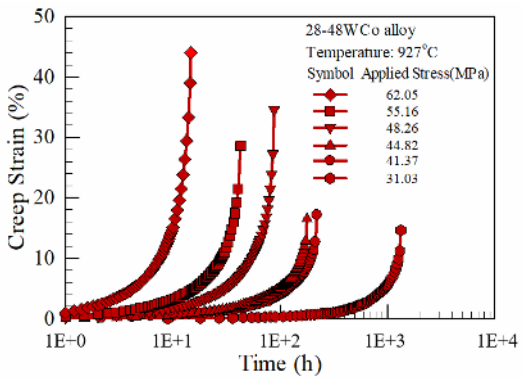

(c)

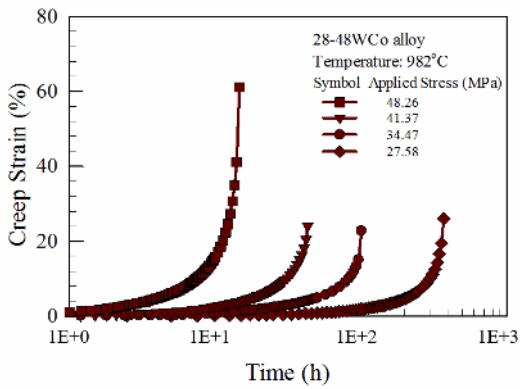

(d)

Fig. 4. Creep test results of the 28-48WCo: (a) At 817 °C; (b) at 871 °C; (c) at 927 °C; (d) at 982 °C.

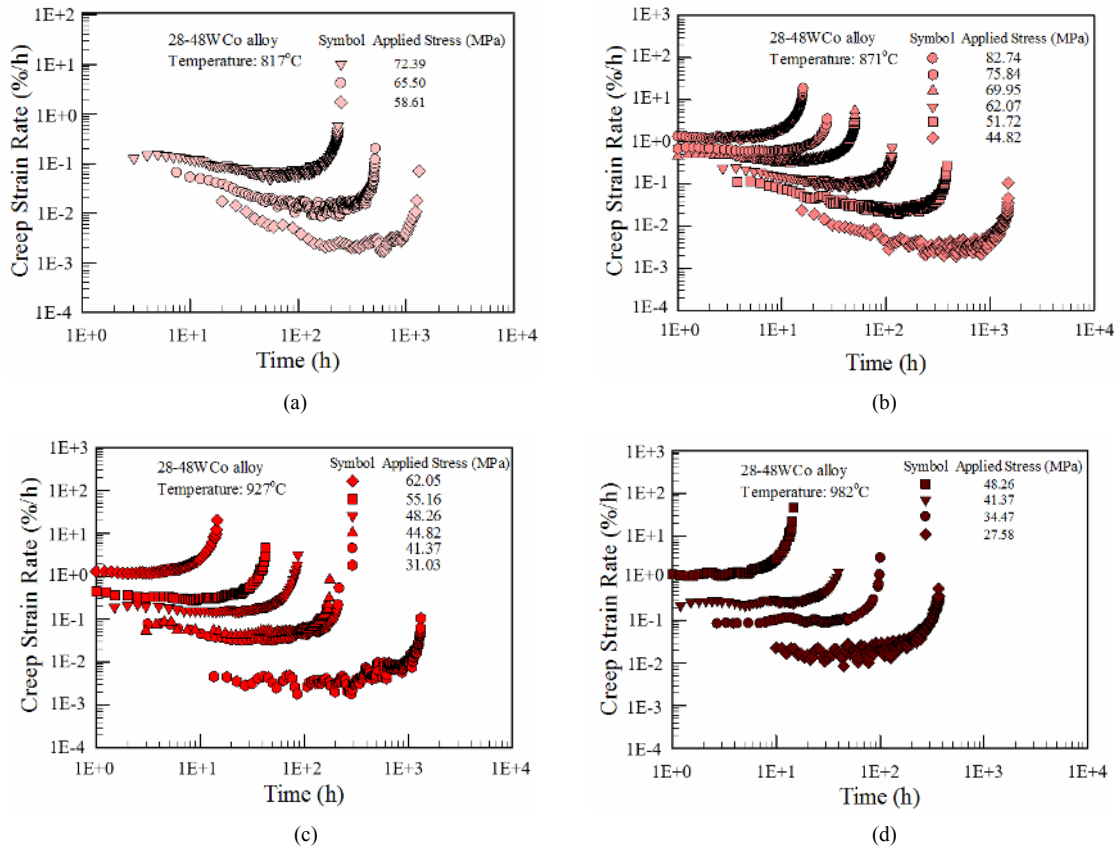

Fig. 5. Creep strain rate versus elapsed time for 28-48WCo alloy: (a) At 817 °C; (b) at 871 °C; (c) at 927 °C; (d) at 982 °C.

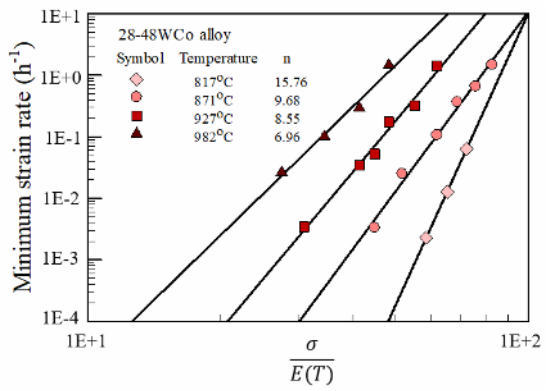

Fig. 6. Minimum strain rate as a function of the applied stress at different test temperature for 28-48WCo alloy steel.

as shownbelow [6, 23]:

$$\dot{\varepsilon} = f(\sigma, T)$$

$$\dot{\varepsilon} = A_0 \left\{ \frac{\sigma}{E(T)} \right\}^n \exp\left[-\frac{Q}{RT} \right]. \quad (2)$$

Here, $\dot{\varepsilon}$ is the minimum creep strain rate, σ is the applied stress, E is the Young's modulus of the material, R is the universal gas constant, T is the absolute temperature, and Q is the activation energy for creep. n is the creep exponent. A_0 and n are material constants.

Using the experimental data given in Table 2, the materials constants A_0 and n characterizing stress dependency, and Q characterizing temperature dependency, were determined by a regression method. The error between the experimentally measured minimum creep strain rate values and the values estimated using Eq. (2) was minimized with all the data points.

The determined values of the three constants, A_0, n and Q for Eq. (2) were 7.989×10^{11} h^{-1}, 8.577, and 1.763×10^5 J/mol, respectively. Substituting these values in Eq. (2), the constitutive equation for the minimum creep rate became as follows:

$$\dot{\varepsilon} = 7.989\times10^{11} \left(\frac{\sigma}{E(T)} \right)^{8.577} \exp\left(-\frac{1.763\times10^5}{RT} \right) \quad (3)$$

where $E(T) = -2.7027\times10^{-3}T^2 + 4.4702\times10^{0}T - 1.6409\times10^{3}$ and $R = 8.314$ J/Kmol.

A comparison between the experimentally obtained minimum creep strain rate and the predicted one is shown in Fig. 7. The maximum deviation is found to be 1.632×10^{-2} h^{-1} at 982 °C under 48.26 MPa. The root mean square error (R) in the prediction of minimum creep strain rate was 4.421×10^{-3} h^{-1}. The coefficient of determination (R^2) between the experimental values of the minimum creep rate and predicted minimum

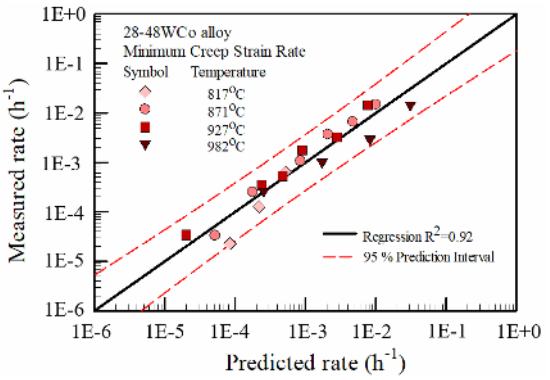

Fig. 7. Comparison between the measured minimum creep strain rate data and predicted values using the Sherby-Dorn creep constitutive model.

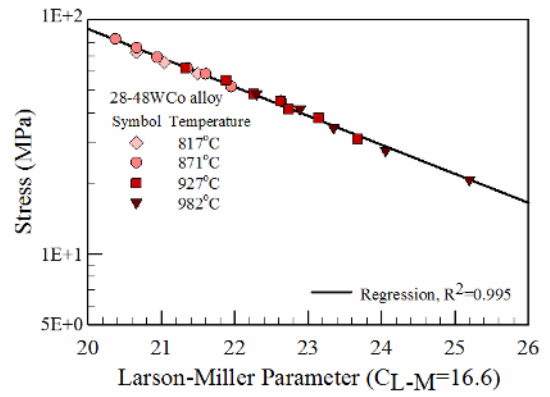

Fig. 8. Creep rupture life curve for the 28-48WCo alloy characterized by the Larson-Miller parameter with $C_{L\text{-}M}$ of 16.6.

creep rate was found to be 0.92. In addition, 95 % confidence band was added in the graph for showing the accuracy of data points. It can be argued that these points are located within the prediction region of 95 % accuracy.

All data points in Fig. 7 were very close to the 45° equivalency line, indicating the good predictability of Eq. (3) in terms of the minimum creep strain rate. Eq. (3) was derived using the data measured at a temperature range of 817-982 °C and under a stress range of 27.58-82.74 MPa. To show the effectiveness of the constitutive equation model, another test was conducted under a condition outside of this range, i.e., at 982 °C and under 20.68 MPa. The measured minimum strain rate was 2.307×10^{-5} h^{-1} and the predicted value was 2.153×10^{-5} h^{-1}. The error was less than −6.7 %.

From the results shown in Fig. 7, it can be argued that the creep strain rate modeled by Sherby and Dorn and the Barrett equation can provide an accurate prediction of the creep deformation behavior for 28-48WCo steel.

3.5 Creep life prediction

The measured creep rupture life results were characterized by the Larson-Miller parameter, expressed as in Eq. (4).

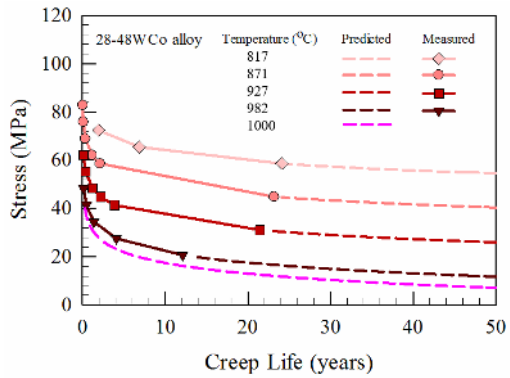

Fig. 9. Creep life prediction curves for various stress and temperature conditions for the 28-48WCo alloy.

$$LMP = (T + 273) \times (C_{L-M} + \log t_r) / 1000 \quad (4)$$

where LMP is the Larson-Miller parameter, t_r is the creep rupture life (h), and T is the temperature in Celsius (°C). Because the numeric values of the *LMP* are dependent on the constant value of $C_{L\text{-}M}$ used in Eq. (4), an optimum value of $C_{L\text{-}M}$ needed to be determined. The value of $C_{L\text{-}M}$ was determined as 16.6 so that the best fit of the data was achieved. The results are shown in Fig. 8. In this figure, all the measured data are shown in a semi-log plot using the *LMP* with $C_{L\text{-}M}$ value of 16.6. A linear relationship between the stress (σ) and the *LMP* was obtained with scatter of $R^2 = 0.995$ as follows:

$$\log\sigma = 335.96 - 11.62 * LMP\,. \quad (5)$$

The creep rupture life curve of the 28-48WCo alloy shown in Fig. 8 was very close to that of Fe-Cr-Ni stainless steel (HP40Nb grade alloy) reported by Voicu et al. [24] and by Roy et al. [25]. As they used different values of $C_{L\text{-}M}$, 15.0 and 22.9, respectively, the creep life curves could not be directly compared with the current data. However, by changing the $C_{L\text{-}M}$ value of the current data to 15.0 and 22.9, comparisons were made. The data almost overlapped with each other, showing little difference, which verifies that the creep lives were almost comparable.

The creep life curve prediction corresponding to the optimum value of $C_{L\text{-}M}$ of 16.6 can be determined from Eqs. (4) and (5). The plots in Fig. 9 depict the trend of the remaining creep lives under constant stress and temperature conditions, showing an increased design creep life as stress and temperature decrease. All the experimentally measured creep life data are also shown in the figure. Fig. 9 can be used to estimate the creep life of the 28-48WCo alloy in the temperature range of 817-982 °C. The dotted lines are curves outside of the creep testing condition of this study.

4. Conclusions

The creep deformation behavior and creep rupture life of

the 28-48WCo alloy were studied by conducting a series of experimental creep tests under temperature conditions of 817, 871, 927 and 982 °C and under stress conditions of 27.58 to 82.74 MPa. The following conclusions were obtained.

(1) The Norton's power law creep exponent n value was decreased from 15.76 to 6.96 as the testing temperature increased from 817 °C to 982 °C. The creep constitutive equation was modeled using the Sherby-Dorn equation, considering the dependency of creep deformation on the temperature and applied stress. This model provided good predictability of the minimum creep strain rate in the range of the experimental test condition, with a coefficient of determination of 0.92.

(2) The creep rupture life was successfully characterized using the Larson-Miller parameter. Creep life design curves were proposed to estimate the creep life of the 28-48WCo alloy in the temperature range of 817-982 °C.

Acknowledgments

This study was supported by the KETEP (No. 2014 1010 101850) and KIAT (No. N0001075), with financial resources granted by the Ministry of Trade, Industry & Energy (MOTIE), Republic of Korea.

Nomenclature

E	: Young's modulus
A_0	: Material constant
n	: Creep exponent
$\dot{\varepsilon}$	: Strain rate
σ	: Applied stress
Q	: Activation energy for creep
R	: Universal gas constant
R	: Root mean square error
R^2	: Coefficient of determination
T	: Temperature

References

[1] T. Zengwu, L. Jinshan, H. Rui, L. Yi and B. Guanghai, Effects of solution heat treatment on carbide of Ni-Cr-W superalloy, *Rare Metal Materials and Engineering*, 39 (7) (2010) 1157-1161.

[2] M. Mostafaei, M. Shamanian, H. Purmohamad, M. Amini and A. Saatchi, Microstructural degradation of two cast heat resistant reformer tubes after long term service exposure, *Engineering Failure Analysis*, 18 (1) (2011) 164-171.

[3] A. P. Gulyaev and I. K. Kupalova, Effect of cobalt on the structure and properties of high-speed steels, *Metal Science and Heat Treatment*, 12 (8) (1970) 666-671.

[4] *https://www.linkedin.com/pulse/21-chemical-elements-effects-steel-mechanical-properties-jeremy-he.*

[5] E. Guglielmino, R. Pino, C. Servetto and A. Sili, Creep damage of high alloyed reformer tubes, *Handbook of materials failure analysis with case studies from the chemicals, concrete and power industries* (2016) 69-91.

[6] C. R. Barrett, A. J. Ardell and O. D. Sherby, Influence of modulus on temperature dependence of activation energy for creep at high temperatures, *Transactions of the Metallurgical Society of AIME*, 230 (1) (1964) 200.

[7] N. C. Z. Htun, T. T. Nguyen, D. Won and K. B. Yoon, Creep fracture behavior of SUS304H steel with vanadium addition based on small punch creep testing, *Material at High Temperature*, 34 (2017) 33-40.

[8] C. Jang, S. H. Kim, I. Sah and D. Kim, Creep behavior of Alloy 617 in high temperature air and helium environments-effect of oxidation damage, *Journal of Mechanical Science and Technology*, 30 (10) (2016) 4433-4438.

[9] T. Yamane, Y. Takahashi and K. Nakagawa, Effect of carbide precipitates on high temperature creep of a 20Cr-25Ni austenitic stainless steel, *Journal of Materials Science Letters*, 3 (6) (1984) 557-559.

[10] A. Ghatak and P. S. Robi, A comparative study of constitutive equations for the creep deformation of HP40Nb microalloyed steel, *Material Science & Engineering A*, 648 (2015) 418-427.

[11] P. Duda, L. Felkowski, J. Dobrzański and H. Purzyńska, Modelling the strain and stress state under creep conditions in P91 steel, *Material at High Temperature*, 33 (1) (2016) 85-93.

[12] J. Christopher and B. K. Choudhary, Applicability of improved Dyson-McLean approach to creep deformation behavior of tempered martensitic P9 steel, *Material at High Temperature* (2017) 1-11.

[13] D. R. Hayhurst, F. Vakili-Tahami and J. Q. Zhou, Constitutive equations for time independent plasticity and creep of 316 stainless steel at 550 °C, *International Journal of Pressure Vessels and Piping*, 80 (2) (2003) 97-109.

[14] R. Mustata and D. R. Hayhurst, Creep constitutive equations for a 0.5 Cr 0.5 Mo 0.25 V ferritic steel in the temperature range 565 C-675°C, *International Journal of Pressure Vessels and Piping*, 82 (5) (2005) 363-372.

[15] W. G. Kim, S. H. Kim and W. S. Ryu, Creep characterization of type 316LN and HT-9 stainless steels by the KR creep damage model, *KSME International Journal*, 15 (11) (2001) 1463-1471.

[16] Y. Zhao, J. Gong, J. Yong, X. Wang, L. Shen and Q. Li, Creep behaviors of Cr25Ni35Nb and Cr35Ni45Nb alloys predicted by modified theta method, *Material Science & Engineering A*, 649 (2016) 1-8.

[17] *http://matweb.com/search/DataSheet.aspx?MatGUID=25b6284c48e0466cb3258c1c8f583b39.*

[18] *Alloy data sheet for KHR48NCo*, Kubota metal corporation (1999).

[19] *ASTM E8/E8M*, Standard test methods for tension testing of metallic materials (2016).

[20] *ASTM E139*, Standard test methods for conducting creep, creep-rupture, and stress-rupture test of metallic materials (2011).

[21] J. Swaminathan, K. Guguloth, M. Gunjan, P. Roy and R.

Ghosh, Failure analysis and remaining life assessment of service exposed primary reformer heater tubes, *Engineering Failure Analysis*, 15 (4) (2008) 311-331.

[22] A. K. Ray, S. K. Sinha, Y. N. Tiwari, J. Swaminathan, G. Das, S. Chaudhuri and R. Singh, Analysis of failed reformer tubes, *Engineering Failure Analysis*, 10 (2003) 351-362.

[23] M. Malu and J. K. Tien, The elastic modulus correction term in creep activation energies: Applied to oxide dispersion strengthened superalloy, *Scr. Metall*, 9 (10) (1975) 1117-1120.

[24] R. Voicu, J. Lacaze, E. Andrieu, D. Poquillon and J. Furtado, Creep and tensile behavior of austenitic Fe-Cr-Ni stainless steels, *Material Science & Engineering A*, 510 (2009) 185-189.

[25] N. Roy, A. Raj, B. N. Roy and A. K. Ray, Creep deformation and damage evaluation of service exposed reformer tube, *Canadian Metallurgical Quarterly*, 54 (2) (2015) 205-222.

Van Hung Dao received his M.S. degree in Mechanical Engineering from Chung-Ang University, Korea in 2016. He is currently a Ph.D. student at Chung-Ang University. His research interests are microstructural analysis and application of high temperature fracture mechanics to life assessment of structural material such as reformer tube.

Kee Bong Yoon received his M.S. in Mechanical Engineering from KAIST and Ph.D. from Georgia Institute of Technology. He is currently a Professor at Chung-Ang University. His research interests are high temperature fracture mechanics, failure analysis and risk based management of facilities in semiconductor industry as well as the conventional power and process plants.

Gimo Yang received his Ph.D. degree in Mechanical Engineering from Chung-Ang University, Korea in 2014. Dr. Yang is currently a Director of engineering at MetalLAB, Inc. His research interest is engineering failure analysis and diagnosis of plant and process facilities.

Jae Sung Oh received his M.S. in Industrial System Engineering from Chungnam National University. He is currently a Ph.D. candidate in Chung-Ang University. And he is also President in MetalLAB Inc. His research interests are mechanical behavior of dissimilar weldments in power and process plant.